Electronic Supplementary Material (ESI) for Dalton Transactions.

Supporting Information

Ce-doping induces bimetallic phosphide heterostructure rapid electron transfer to achieve efficient hydrogen production

Maobin Wang, [1] *Zhaochen Liu,* [2] *Shiyu Guo,* [1] *Wenzhe Liu,*[1] *Changpeng Ji,* [1] *Lu Wang,* [3] *Daohong Yao* [4*]

[1]*College of Mechanical and Electronic Engineering, Qingdao University of Technology, Qingdao 266520, PR China*

[2]*College of Civil and Architectural Engineering, Qingdao University of Technology, Qingdao 266520, PR China*

[3]*College of Management Engineering, Qingdao University of Technology, Qingdao 266520, PR China*

[4]*College of Basic Courses Department, Qingdao University of Technology, Qingdao 266520, PR China*

***Corresponding author:** Daohong Yao

E-mail: yaodaohong@qut.edu.cn

Phone: +86-23-5797008;

Address: College of Basic Courses Department, Qingdao University of Technology, Qingdao 266520, PR China

1.1. Chemical materials

$Fe(NO_3)_3·9H_2O$ (98.5 wt%), $Ni(NO_3)_2·6H_2O$ (99.8 wt%), $Ce(NO_3)_4$ (99.9 wt%), urea (＞99 wt%), NH_4F (99 wt%), NaH_2PO_2 (99.0 wt%) and nickel foams (NFs) (99.9 wt%) were purchased from Shanghai McLean Biochemical Technology Co., Ltd, Chengdu Kelong Chemical Co., Ltd, Titan Technology Co. Ltd (China), Beijing Mairuida Technology Co., Ltd, Aladdin and Kunshan Guangjiayuan New Materials Co., Ltd. Considering the compounds utilized in this study were of analytical quality, no additional purification was required.

1.2. Preparation of NiFe-LDH@NF, Fe-LDH@NF and Ni-LDH@NF electrodes

1.00 mmol of $Ni(NO_3)_2·6H_2O$, 1.00 mmol of $Fe(NO_3)_3·9H_2O$, 6.00 mmol of urea, and 1.00 mmol of NH_4F were dissolved in 30 mL of deionized water to form a yellow green solution. The treated NF and the resulting solution were then put into a 50 mL polytetrafluoroethylene lined stainless steel autoclave and kept at 120 °C for 8 hours, after which the precursor NiFe-LDH@NF was collected; 1.00 mmol of $Fe(NO_3)_3·9H_2O$, 6.00 mmol of urea, and 1.00 mmol of NH_4F were dissolved in 30 mL of deionized water to form a yellow green solution. The treated NF and the resulting solution were then put into a 50 mL polytetrafluoroethylene lined stainless steel autoclave and kept at 120 °C for 8 hours, after which the precursor Fe-LDH@NF was collected; 1.00 mmol of $Ni(NO_3)_2·6H_2O$, 6.00 mmol of urea, and 1.00 mmol of NH_4F were dissolved in 30 mL of deionized water to form a yellow green solution. The treated NF and the resulting solution were then put into a 50 mL polytetrafluoroethylene lined stainless steel autoclave and kept at 120 °C for 8 hours, after which the precursor Ni-

LDH@NF was collected. All samples were washed with deionized water several times, and vacuum dried at 60 °C overnight.

1.3. Preparation of NiFeP@NF, Fe_2P@NF and NiP_2@NF electrodes

NiFe-LDH@NF, Fe-LDH@NF and Ni-LDH@NF were transformed to NiFeP@NF, Fe_2P@NF and NiP_2@NF by the phosphating procedure. Place 0.5 g of NaH_2PO_2 and the LDH precursor at opposite ends of the tube furnace, with the NaH_2PO_2 upstream and the precursor 5 cm downstream. The phosphating procedure is carried out for 2 hours in an argon environment at 350 °C at a heating rate of 5 °C min^{-1}. In addition, a similar method was used to create the NiFeP@NF, Fe_2P@NF and NiP_2@NF electrodes.

1.4. Different Ce doping NiFeP@NF electrodes

1.00 mmol of $Ni(NO_3)_2\cdot 6H_2O$, 1.00 mmol of $Fe(NO_3)_3\cdot 9H_2O$, $Ce(NO_3)_4$, 6.00 mmol of urea, and 1.00 mmol of NH_4F were dissolved in 30 mL of deionized water to form a yellow green solution. Here, The amount of $Ce(NO_3)_4$ added has three types (0.05 mmol denoted as 1, 0.2 mmol denoted as 2, 0.5 mmol denoted as 3). The treated NF and the three different Ce doping solutions were then put into a 50 mL polytetrafluoroethylene lined stainless steel autoclave and kept at 120 °C for 8 hours, collecting three LDH precursors. All samples were washed with deionized water several times, and vacuum dried at 60 °C overnight. The subsequent phosphating conditions are the same as above. Ce-NiFeP@NF-1, Ce-NiFe-LDH@NF-2, and Ce-NiFeP@NF-3 were collected.

1.5. Characterization of Materials

Analyzing the phase composition included using X-ray diffraction (XRD) on PANalytical X'Pert powder (PANalytical B.V.). Transmission electron microscopy (TEM, FEI Talos F200S) and environmental scanning electron microscopy (ESEM, FEI Quattro s) were used to analyze the microstructure and morphology of the synthesized electrocatalysts, respectively. High angle annular dark field scanning TEM (HAADF-STEM) and energy dispersive X-ray (EDX) spectroscopy were used to analyze the element distribution of common catalysts. The X-ray photoelectron spectroscopy (XPS) experiments were recorded on a Thermo SCIENTIFIC ESCALAB 250 Axis Ultra spectrometer using a monochromatic Al Kα ($h\nu$= 1486.6 eV).

1.6. Electrochemical Measurements

All the HER and OER catalytic performances were investigated on the CHI660E electrochemical workstation (Chenhua, Shanghai) with a typical three-electrode system at 25 °C. A piece of treated Ni foam (1 cm ×1.5 cm) was used as the working electrode, and saturated calomel electrode (SCE) and graphite rod were used as reference electrode and counter electrode, respectively. The OER and HER activities were evaluated by using linear sweep voltammetry (LSV) technique at a scan rate of 5 $mV\bullet s^{-1}$ after 30 cyclic voltammetry (CV) testing in 1.0 M KOH electrolyte. Also, Tafel curves were measured at a scan rate of 0.1 mV/s. Electrochemical impedance spectroscopy (EIS) measurements were undertaken with an amplitude of 0.01 V throughout a frequency range of 0.01Hz to 100kHz. Setting the overpotential in Tafel plots to zero can easily yield the exchange current density (j_0) of catalysts. The double layer capacitance (C_{dl}) was measured at different scan rates (5-40 $mV\bullet s^{-1}$) in the non-faraday region (CV). All tested potentials (E_{SCE}) were converted to the reversible hydrogen electrode (E_{RHE}) refer to the equation:

$$E_{RHE} = E_{SCE} + 0.242 + 0.059 \times pH$$

1.7. Calculation of the turnover frequency (TOF)

The turnover frequencies were calculated with the following equation：

$$TOF = \frac{jA1}{Fn2}$$

where A is the electrode's geometrical area, F is the Faradaic constant (96500 C•mol^{-1}), and n represents the mole of the active species during the OER (n=4) or HER (n=2) process. where j is the observed current density at the specified overpotential. By taking into account the fact that two electrons are needed to create one hydrogen molecule from two protons, the factor 1/2 is mentioned.

1.8. Computational details and methods

All the spin-polarized density functional theory (DFT) calculations within the Hubbard U approach (DFT+U) were performed using the Vienna ab initio simulation package (VASP) with a generalized gradient approximation (GGA) based on exchange-correlation function parameterizations including Perdew, Burke, and Ernzerhof (PBE) [4].

The Gamma-centered Monkhorst-Pack grid with (3 × 3 × 1) k-point sampling was used for all systems. The cut-off plane wave basis was set to 500 eV. The standard settings for electronic structure iterations are 1×10^{-5} eV and 0.001 eV Å^{-1}. Various potential adsorption sites were taken into account in the calculations, while only the most stable binding sites were chosen as the real active sites due to the different adsorption energies on different sites.

The formation energy (ΔE_f) per atom of all systems were calculated by [6]:

$$\Delta E_f = (E_{sys}-N_P\times\mu_P-N_{Ni}\times\mu_{Ni}-N_{Fe}\times\mu_{Fe}-N_{Ce}\times\mu_{Ce})/(N_P+N_{Ni}+N_{Fe}+N_{Ce})$$

where the E_{sys} was the total energy of systems, μ_P, μ_{Ni}, μ_{Ce} and μ_{Fe} denoted the chemical potentials of P, Ni, Ce and Fe atoms, using the energy of per atom in their bulk, N_P, N_{Ni}, N_{Fe}, and N_{Ce} were the number of P, Ni, Fe and Ce atoms in systems.

Supplementary Figures

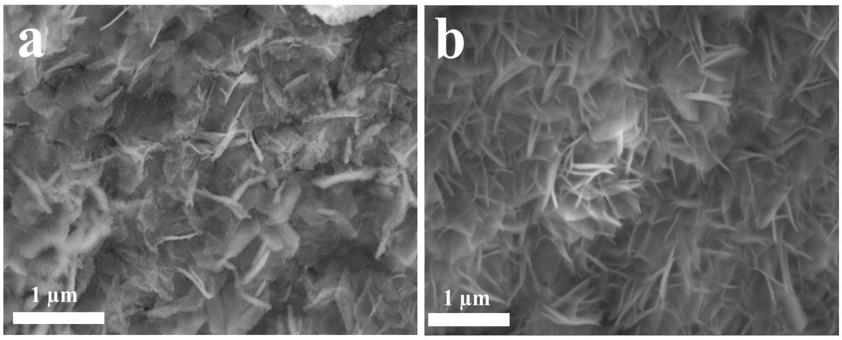

Figure S1. (a) SEM image of NiFe-LDH@NF; (b) SEM image of Ce-NiFe-LDH@NF.

Figure S2. (a) SEM image of Fe_2P@NF; (b) SEM image of NiP_2@NF; (c) SEM image of NiFeP@NF.

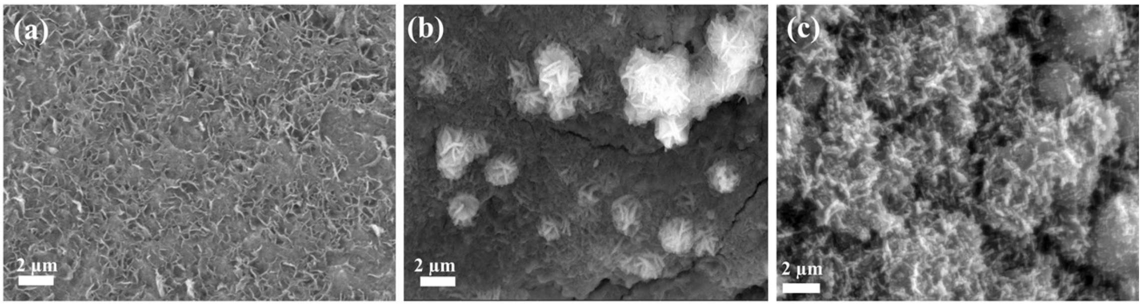

Figure S3. SEM images of (a) Ce-NiFeP@NF-1; (b) Ce-NiFeP@NF-2; (c) Ce-NiFeP@NF-3.

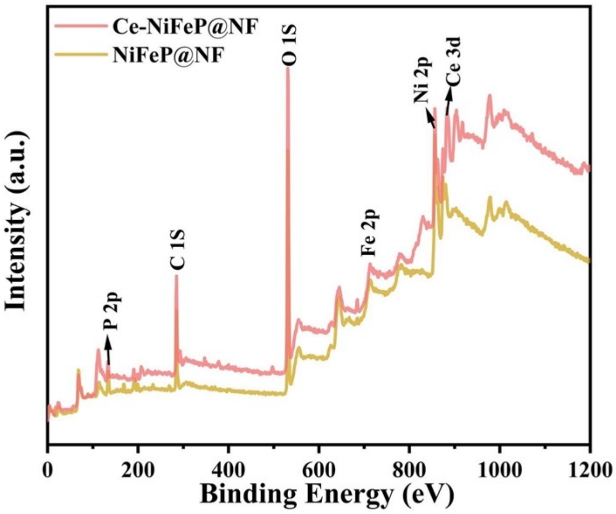

Figure S4. XPS survey spectrum of Ce-NiFeP@NF and NiFeP@NF.

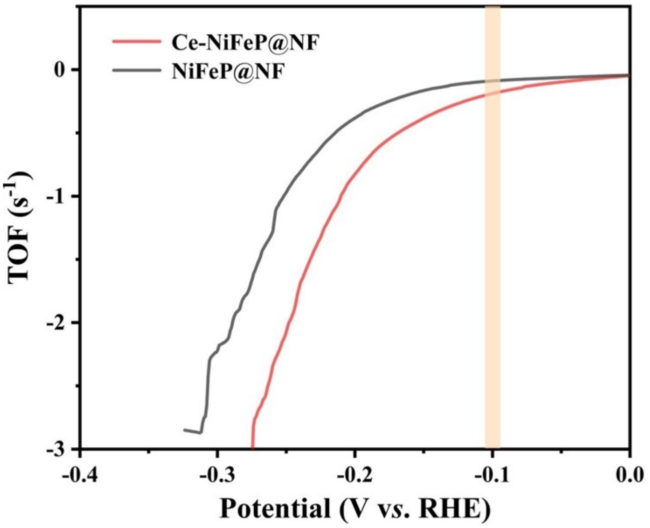

Figure S5. Comparison of TOF at overpotentials of 100 mV for Ce-NiFeP@NF and NiFeP@NF.

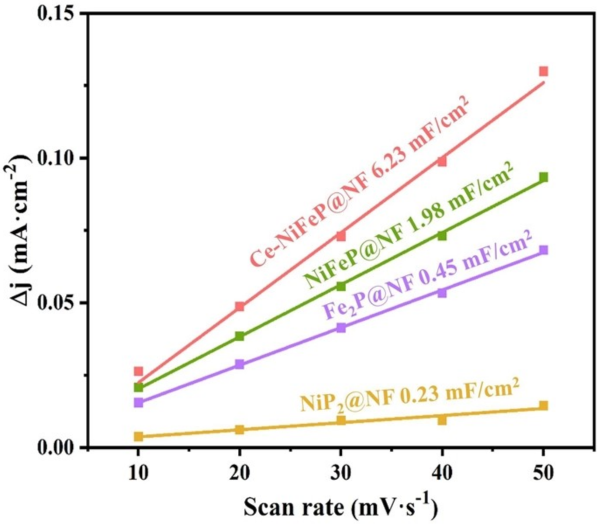

Figure S6. Capacitive currents on the basis of the scan rate for Ce-NiFeP@NF, NiP$_2$@NF, Fe$_2$P@NF, and NiFeP@NF.

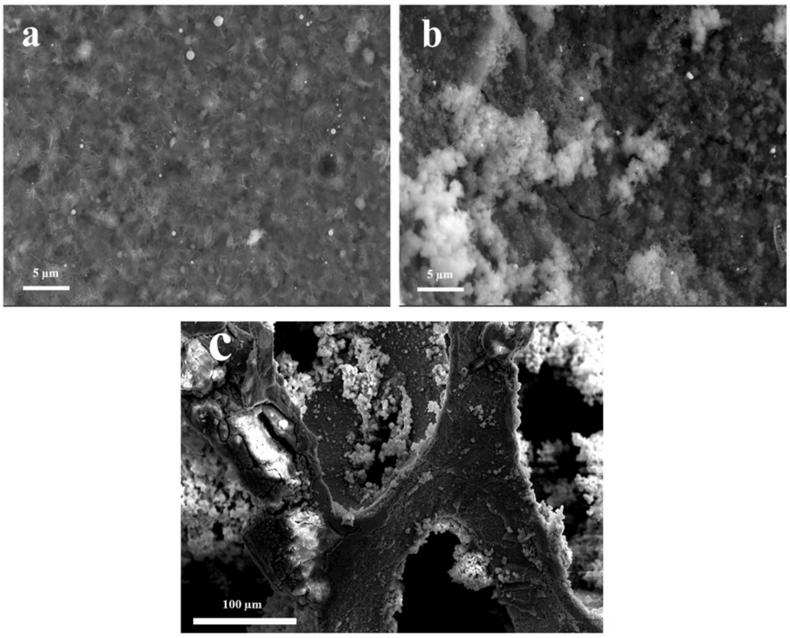

Figure S7. SEM images of Ce-NiFeP@NF after HER test.

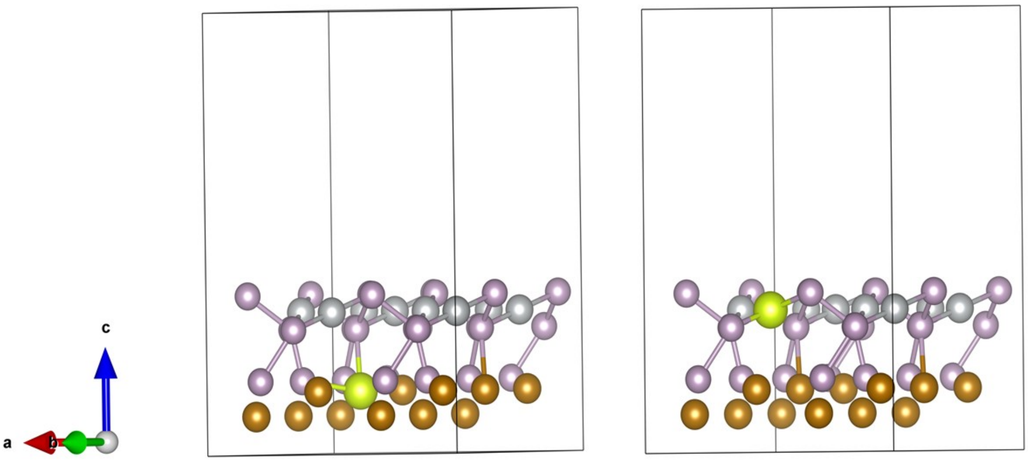

Figure S8. The model and corresponding formation energy of the (a) Fe site; (b) Ni site (grey ball: Ni atom; yellow ball: Fe atom; green ball: Ce atom; purple ball: P atom).

Supplementary tables

Table S1. Comparison of HER performance of Ce-NiFeP@NF with reported electrocatalysts in 1.0 M KOH

Electrocatalysts	**Overpotential (mV) at 10 mA·cm^{-2}**	**Tafel slope (mV dec^{-1})**	**References**
Ce-NiFeP@NF	120	88.7	This Work
$Ni_{0.7}Fe_{0.3}S_2$	155	109	[2]
Co_9S_8@MoS_2	143	117	[3]
CoPS@NPS-C	191	106	[4]
Ni_3S_2/NF	223	-	[5]
FeP nanorod array	218	146	[6]
NiFe Nanotube	181	147	[7]
$Zn_{0.975}Co_{0.025}S/CoS_2$	152	103	[8]
3D-rGO-CeO_2	192	112.8	[9]
$NiCo_2S_4$/NF	210	58.9	[10]
Co_2B	233	92.5	[11]

Table S2. Comparison of overall water splitting performance of Ce-NiFeP@NF with reported materials in 1 M KOH.

Electrocatalysts	Cell voltage (V) at 10 mA·cm^{-2}	References
Ce-NiFeP@NF	1.54	This Work
Mo-Co_9S_8@C	1.56	[19]
Mo-$NiCo_2O_4$/$Co_{5.47}N$	1.56	[16]
Ir-VG	1.57	[21]
Ni/$Ni(OH)_2$ nanosheets	1.59	[20]
Co-Ni-M@CeO_2	1.60	[22]
Co_3O_4-C@FeMoP	1.61	[29]
CeO_2-$Co(OH)_2$	1.62	[23]
NiFe NTAS-NF	1.62	[7]
Ni-Mo_2C	1.64	[24]
MoS_2/Ni_3S_2	1.65	[25]
RuO_2/Co_3O_4-RuCo@NC	1.66	[26]
FeCo/Co_2P	1.68	[27]
NiCo/$NiCoO_x$	1.74	[28]

Reference

[1] P.E. Blochl, Projector augmented-wave method, Phys. Rev. B, 50 (1994), pp. 17953-17979.

[2] J. Yu, G. Cheng, W. Luo, Ternary nickel–iron sulfide microflowers as a robust electrocatalyst for bifunctional water splitting, J. Mater. Chem., 5 (30) (2017), pp. 15838-15844.

[3] J. Bai, T. Meng, D. Guo, S. Wang, B. Mao, M. Cao, Co_9S_8@MoS_2 core-shell heterostructures as trifunctional electrocatalysts for overall water splitting and Zn-air batteries, ACS Appl. Mater. Interfaces, 10 (2018), pp. 1678-1689.

[4] Y.P. Hu, F. Li, Y. Long, H.D. Yang, L.L. Gao, X.F. Long, H.G. Hu, N. Xu, J. Jin, J.T. Ma, Ultrafine CoPS nanoparticles encapsulated in N, P, S tri-doped porous carbon as an efficient bifunctional water splitting electrocatalyst in both acid and alkaline solution, Acc. Chem. Res., 51 (2018), pp. 2857-2866.

[5] L. Feng, G. Yu, Y. Wu, G. Li, H. Li, Y. Sun, T. Asefa, W. Chen, X. Zou, High-index faceted Ni_3S_2 nanosheet arrays as highly active and ultrastable electrocatalysts for water splitting, J. Am. Chem. Soc., 137 (2015), p. 14023.

[6] Y. Liang, Q. Liu, A.M. Asiri, X. Sun, Y. Luo, Self-supported FeP nanorod arrays: a cost-effective 3D hydrogen evolution cathode with high catalytic activity, ACS Catal., 4 (2014), pp. 4065-4069.

[7] L. Xu, F.T. Zhang, J.H. Chen, X.Z. Fu, R. Sun, C.P. Wong, Amorphous NiFe nanotube arrays bifunctional electrocatalysts for efficient electrochemical overall water splitting, ACS Appl. Energy Mater., 1 (2018), pp. 1210-1217.

[8] Z. Yu, Y. Bai, S. Zhang, Y. Liu, N. Zhang, K. Sun, Metal-organic framework-derived $Zn_{0.975}Co_{0.025}S/CoS_2$ embedded in N,S-codoped carbon nanotube/nanopolyhedra as an efficient electrocatalyst for overall water splitting, J. Mater. Chem., 6 (2018), pp. 10441-10446.

[9] M. Liu, Z. Ji, X. Shen, H. Zhou, J. Zhu, X. Xie, C. Song, X. Miao, L. Kong, G. Zhu, An electrocatalyst for a hydrogen evolution reaction in an alkaline medium: three-dimensional graphene supported CeO_2 hollow microspheres, Eur. J. Inorg. Chem., 22 (2018), pp. 3952-3959.

[10] A. Sivanantham, P. Ganesan, S. Shanmugam, Hierarchical $NiCo_2S_4$ nanowire arrays supported on Ni foam: an efficient and durable bifunctional electrocatalyst for oxygen and hydrogen evolution reactions, Adv. Funct. Mater., 26 (2016), pp. 4661– 4672.

[11] J. Masa, P. Weide, D. Peeters, I. Sinev, W. Xia, Z. Sun, C. Somsen, M. Muhler, W. Schuhmann, Amorphous cobalt boride (Co_2B) as a highly efficient nonprecious catalyst for electrochemical water splitting: oxygen and hydrogen evolution, Adv. Energy Mater., 6 (2016), Article 1502313.

[12] X. Yi, X. He, F. Yin, B. Chen, G. Li, H. Yin, Co-CoO-Co_3O_4/N-doped carbon derived from metal-organic framework: the addition of carbon black for boosting oxygen electrocatalysis and Zn-Air battery, Electrochim. Acta, 295 (2019), pp. 966-977.

[13] W. Gao, W. Gou, R. Wei, X. Bu, Y. Ma, J.C. Ho, In situ electrochemical conversion of cobalt oxide@MOF-74 core-shell structure as an efficient and

robust electrocatalyst for water oxidation, Appl. Mater. Today., 21 (2020), p. 100820.

[14] D. Zhao, H. Liu, X. Wu, Bi-interface induced multi-active $MCo_2O_4@MCo_2S_4@PPy$ (M=Ni, Zn) sandwich structure for energy storage and electrocatalysis, Nano Energy, 57 (2019), pp. 363-370.

[15] T. Tang, W.J. Jiang, S. Niu, N. Liu, H. Luo, Q. Zhang, W. Wen, Y.Y. Chen, L.B. Huang, F. Gao, J.S. Hu, Kinetically controlled coprecipitation for general fast synthesis of sandwiched metal hydroxide nanosheets/graphene composites toward efficient water splitting, Adv. Funct. Mater., 28 (2018), Article 1704594.

[16] W. Liu, L. Yu, R. Yin, X. Xu, J. Feng, X. Jiang, D. Zheng, X. Gao, X. Gao, W. Que, P. Ruan, F. Wu, W. Shi, X. Cao, Non-3d metal modulation of a 2D Ni-Co heterostructure array as multifunctional electrocatalyst for portable overall water splitting, Small, 16 (2020), pp. 1-8.

[17] Q. Wang, H. Zhao, F. Li, W. She, X. Wang, L. Xu, H. Jiao, Mo-doped Ni_2P hollow nanostructures: highly efficient and durable bifunctional electrocatalysts for alkaline water splitting, J. Mater. Chem. A, 7 (2019), pp. 7636-7643.

[18] Y. Gong, Z. Yang, Y. Lin, J. Wang, H. Pan, Z. Xu, Hierarchical heterostructure $NiCo_2O_4@CoMoO_4$/NF as an efficient bifunctional electrocatalyst for overall water splitting, J. Mater. Chem. A, 6 (2018), pp. 16950-16958.

[19] L. Wang, X. Duan, X. Liu, J. Gu, R. Si, Y. Qiu, Y. Qiu, D. Shi, F. Chen, X. Sun, Atomically dispersed Mo supported on metallic Co_9S_8 nanoflakes as an

advanced noble-metal-free bifunctional water splitting catalyst working in universal PH conditions, Adv. Energy Mater., 10 (2020), Article 1903137.

[20] L. Dai, Z.N. Chen, L. Li, P. Yin, Z. Liu, H. Zhang, Ultrathin Ni(0)-embedded $Ni(OH)_2$ heterostructured nanosheets with enhanced electrochemical overall water splitting, Adv. Mater., 32 (2020), Article 1906915,

[21] S.B. Roy, K. Akbar, J.H. Jeon, S.-K. Jerng, L. Truong, K. Kim, Y. Yi, S.-H. Chun, Iridium on vertical graphene as an all-round catalyst for robust water splitting reactions, J. Mater. Chem. A, 7 (2019), pp. 20590-20596,

[22] G. Ma, X. Du, X. Zhang, Selective sulfuration, phosphorization and selenylation: a universal strategy toward Co-Ni-M@CeO_2/NF (M = O, S, P and Se) interface engineering for efficie,nt water splitting electrocatalysis, J. Alloy. Compd., 864 (2021), Article 158486.

[23] M. Chen, Y. Lv, P. Wu, L. Dong, X. He, L. Cui, The electron engineering of $CeO_2/Co(OH)_2$ hybrids to enhance the performance for overall water splitting in alkaline media, J. Electroanal. Chem., 918 (2022), Article 116452.

[24] R. Ge, J. Zhao, J. Huo, J.Qu, J. Yang, Y. Li, M. Zhu, J.M. Cairney, R. Zheng, S. Li, J. Zhang, B. Liu, W. Li, Multi-interfacial Ni/Mo_2C ultrafine hybrids anchored on nitrogen-doped carbon nanosheets as a highly efficient electrocatalyst for water splitting, Mater. Today Nano, 20 (2022), Article 100248.

[25] X.L. Liu, P. Wang, Q.Q. Zhang, B.B. Huang, Z.Y. Wang, Y.Y. Liu, Z.K. Zheng, Y. Dai, X.Y. Qin, X.Y. Zhang, Synthesis of MoS_2/Ni_3S_2 heterostructure for

efficient electrocatalytic hydrogen evolution reaction through optimizing the sulfur sources selection, Appl. Surf. Sci., 459 (2018), pp. 422-429.

[26] Z. Fan, J. Jiang, L. Ai, Z. Shao, S. Liu, Rational design of ruthenium and cobalt-based composites with rich metal–insulator interfaces for efficient and stable overall water splitting in acidic electrolyte, ACS Appl. Mater. Interfaces, 11 (2019), pp. 47894-47903.

[27] Q. Shi, Q. Liu, Y. Ma, Z. Fang, Z. Liang, G. Shao, B. Tang, W.Y. Yang, L. Qin, X.S. Fang, High-performance trifunctional electrocatalysts based on FeCo/Co_2P hybrid nanoparticles for zinc-air battery and self-powered overall water splitting, Adv. Energy Mater., 10 (2020), p. 1903854.

[28] Y. Shao, M. Zheng, M. Cai, L. He, C. Xu, Improved electrocatalytic performance of core-shell NiCo/$NiCoO_x$ with amorphous FeOOH for oxygen-evolution reaction, Electrochim. Acta, 257 (2017), pp. 1-8.

[29] A.Z. Alhakemy, N. Senthilkumar, Y. Ding, J. Li, Z. Wen, Co_3O_4-C@FeMoP on nickel foam as bifunctional electrocatalytic electrode for high-performance alkaline water splitting, Int. J. Hydrogen Energy, 46 (2021), pp. 32846-32857.